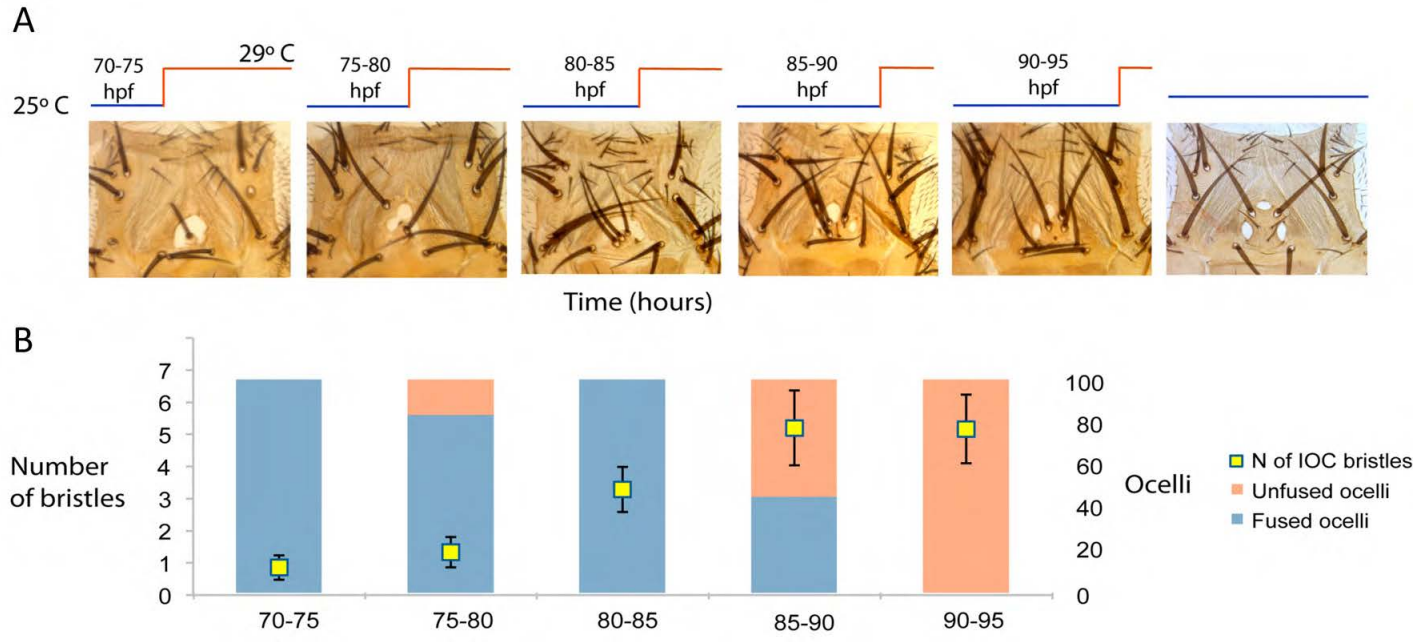

Fig. S1. Temporal requirement of *Dl/Notch* signaling for interocellar fate establishment. (**A**) Five-hour collections of *oc2>Dl-RNAi* embryos were grown at 25°C and shifted to 29°C at different developmental times as indicated. Representative views of the ocellar complex are shown. Maintenance of the culture at 25°C results in wild-type flies (last panel). Shifted animals develop macrobristles in the interocellar region, instead of the normal microbristles in the wild type. This is probably due to precocious bristle differentiation in the absence of *Dl* signaling, independent of the earlier role in interocellar fate specification of *Dl*. (**B**) Quantification of the number of interocellar bristles (yellow squares with standard error bars). Rectangles represent the percentage of flies with fused (cyclopic) and unfused ocelli. After 85 hpf, the interocellar region becomes *Dl/Notch* independent.

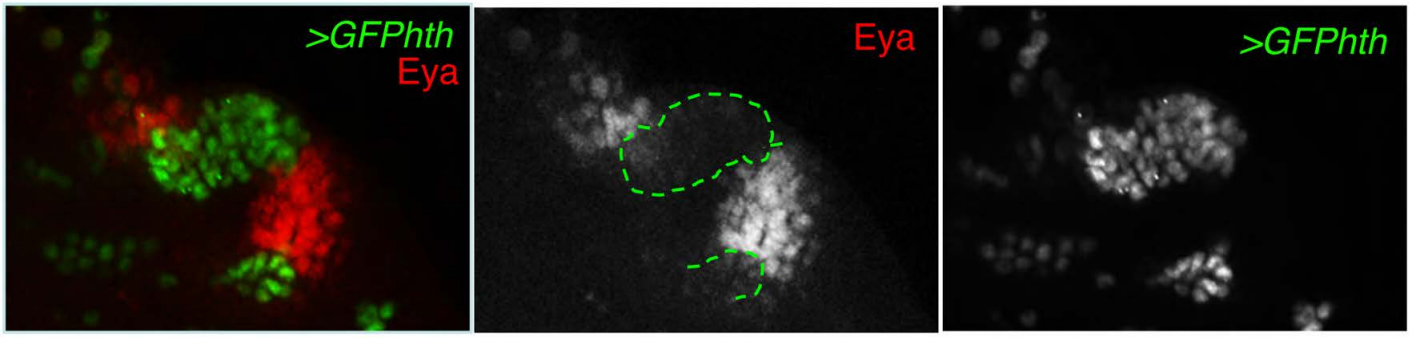

Fig. S2. *hth* represses Eya cell-autonomously. *GFPhth*-expressing clones (green) in the ocellar field, stained for Eya expression. Merged and single channels are shown. *GFPhth* represses *eya* expression cell autonomously. The clones are outlined on the Eya channel.

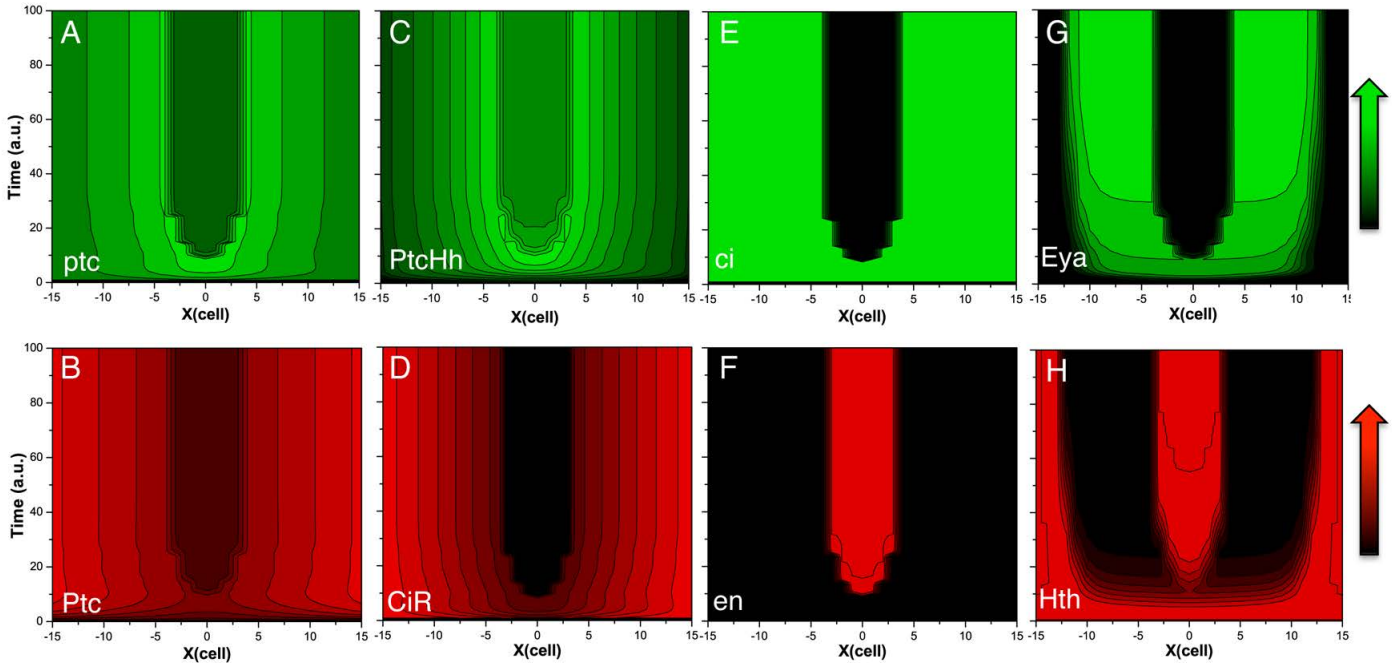

Fig. S3. Spatiotemporal dynamics of model variables. Surface contour plots showing the spatiotemporal patterns of model variables not described in Fig. 6. Capitalized names indicate protein products, whereas non-capitalized names indicate transcript species. a.u., arbitrary units. Cell number is represented on the *x* axis.

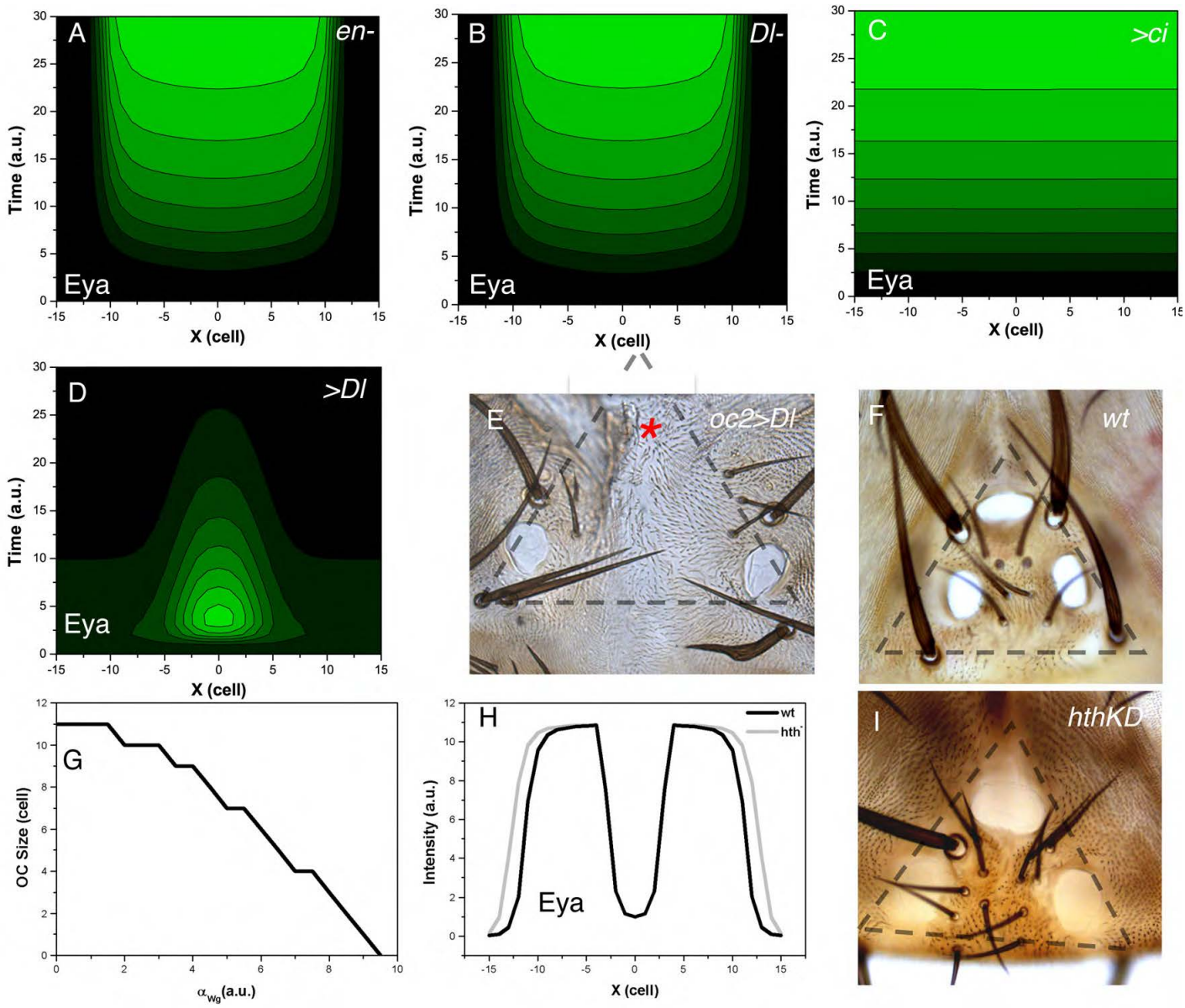

Fig. S4. Analaysis of mutant genotypes. (**A-D**) Spatiotemporal dynamics of Eya expression predicted in modeled mutants, as indicated in each panel. To mimic loss of function mutations in *en*, *Dl* and *hth*, the following parameters values were used: θ_{en}=0; k_{DlEn}=2; α_{Wghth}=0, respectively. The overexpression of *ci* and *Dl* were modeled by increasing the *ci* basal transcription rate (α_{ci}=6) and by reducing k_{DlEn} (k_{DlEn}=0.1), respectively. Simulations of *en* (A) and *Dl* (B) loss reproduce qualitatively the results shown in Fig. 3C and Fig. 4A,C (expansion of the ocellar/Eya domain and loss of the interocellar region). Overexpression of *ci* (C) results in extended Eya-positive/ocellar tissue, as observed experimentally in Fig. 3G. *Dl* overexpression is predicted to expand the interocellar region at the expense of the Eya-expressing domains (D) (and thereby the ocelli) which, with the parameters used, result in the loss of ocelli. (**E**,**F**) When this prediction is tested in vivo by overexpression of *Dl* driven by *oc2-GAL4* (*oc2>Dl*), the interocellar region expands notably and the anterior ocellus disapears (asterisk). The posterior ocelli are abnormally shaped, but still present (E), suggesting uneven expression of the *oc2-GAL4* driver in the ocellar region or unrecognized biological asymmetries between anterior and posterior ocelli. (**G**) The expression of *hth* is predicted to regulate the size of the ocellar domain, such that as its transcription increases (i.e. increasing α_{Wg}) the ocellar domain (the number of Eya-expressing cells) decreases. (**H**) Therefore, when *hth* transcription is shut off, the Eya domain expands. (**I**) This is indeed what is detected by knocking down in vivo *hth* expression, in *oc2>hthRNAi* ('*hthKD*') individuals. Note the irregular perimeter of the ocelli in this genotype. a.u., arbitrary units.

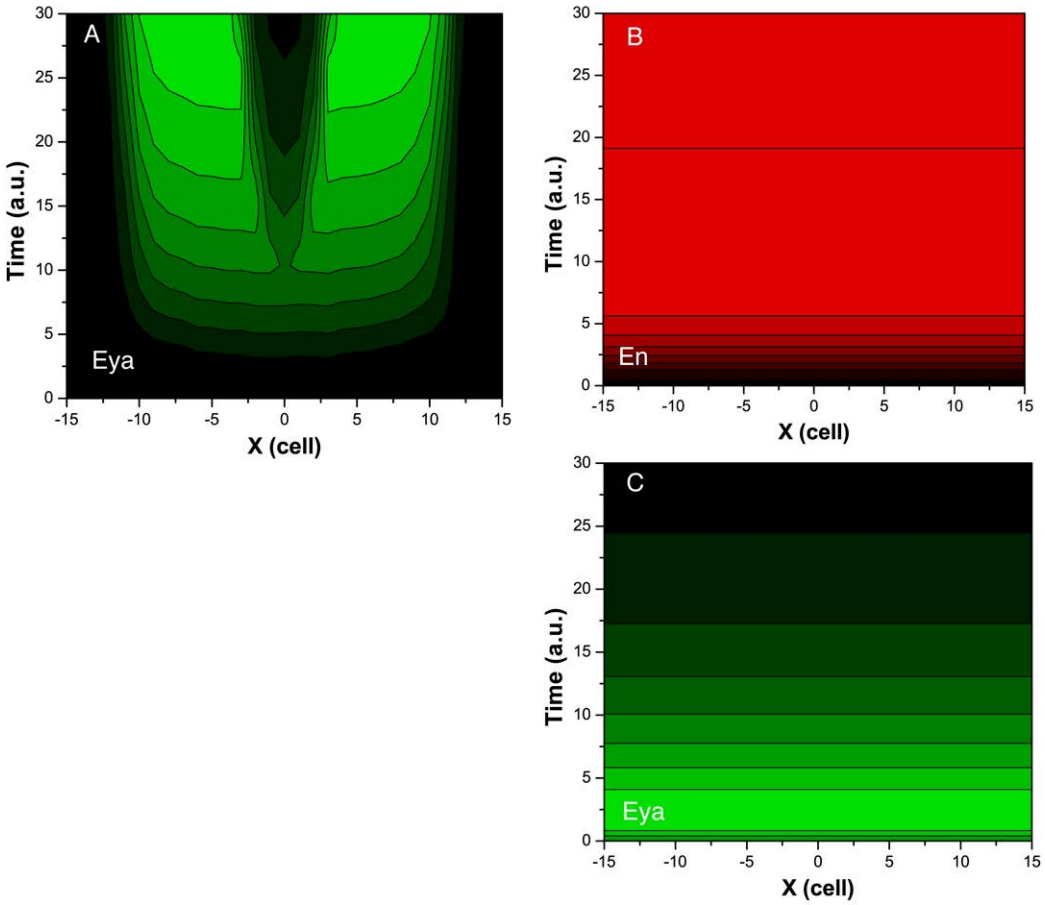

Fig. S5. Convergence to the wild-type pattern with varying initial conditions. Surface contour plots showing the spatiotemporal patterns of model variables. (**A**) Evolution of Eya pattern when the initial value of every system variable was randomized (up to a 10-fold change) in each individual cell. The different initial conditions applied to each cell describe a fluctuating spatiotemporal pattern in the first time steps. These fluctuations are smoothed with time as the system converges to a stable stationary solution. (**B**,**C**) Evolution of En (B) and Eya (C) when the initial condition for En exceeds the concentration determined by the parameter k_{DlEn}, responsible for En autoregulation (k_{DlEn}>0.2).

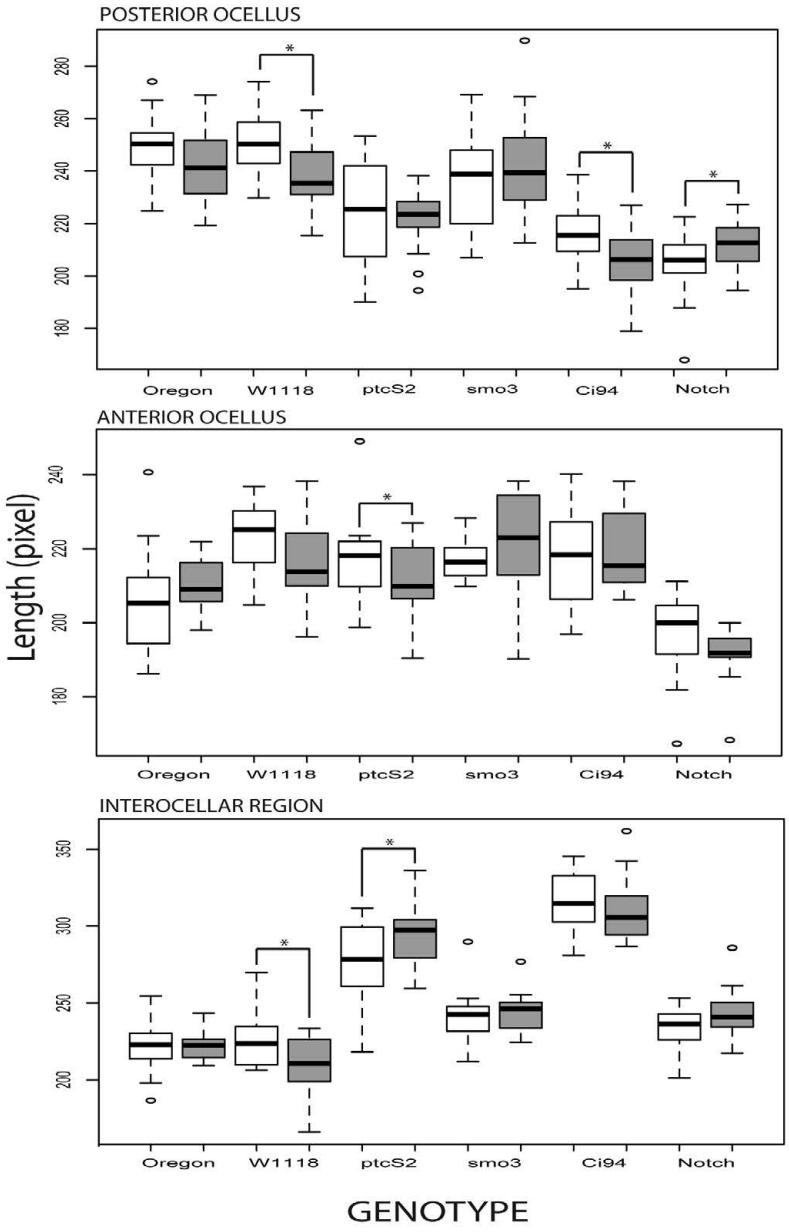

Coefficient of Variation (Cv) expressed in percentage

	Posterior Ocellus		Anterior Ocellus		Interocellar Region	
Oregon/Oregon*	4,72	5,98	3,94	4,39	7,29	4,71
W1118/W1118*	4,84	6,39	6,59	6,84	7,42	8,69
ptcS2/ptcS2*	8,23	5,04	4,98	3,09	11,15	6,48
smo3/smo3*	7,24	7,52	7,05	6,06	7,32	5,05
Ci94/Ci94*	5,23	5,99	4,93	7,27	5,95	6,57
Notch/Notch*	5,97	4,15	4,99	4,99	3,49	6,40

* with temperature cycles

Fig. S6. Quantitative variations in ocellar structures under temperature perturbations. Box plot showing measurements of the posterior ocellus, anterior ocellus and the interocellar region in the indicated genotypes. Length is expressed in pixels. White boxes represent strains grown at constant 25°C whereas gray boxes represent strains subjected to temperature cycles (see Materials and methods). Circles denote outliers above or below the inter-quartile range. Number of measured anterior ocelli, posterior ocelli and interocellar regions is 10, 20 and 20, respectively. Only females were included. Asterisks indicate significant differences between two experimental conditions (P<0.05). Below, the table contains the coefficient of variation within genotypes, expressed in percentage.

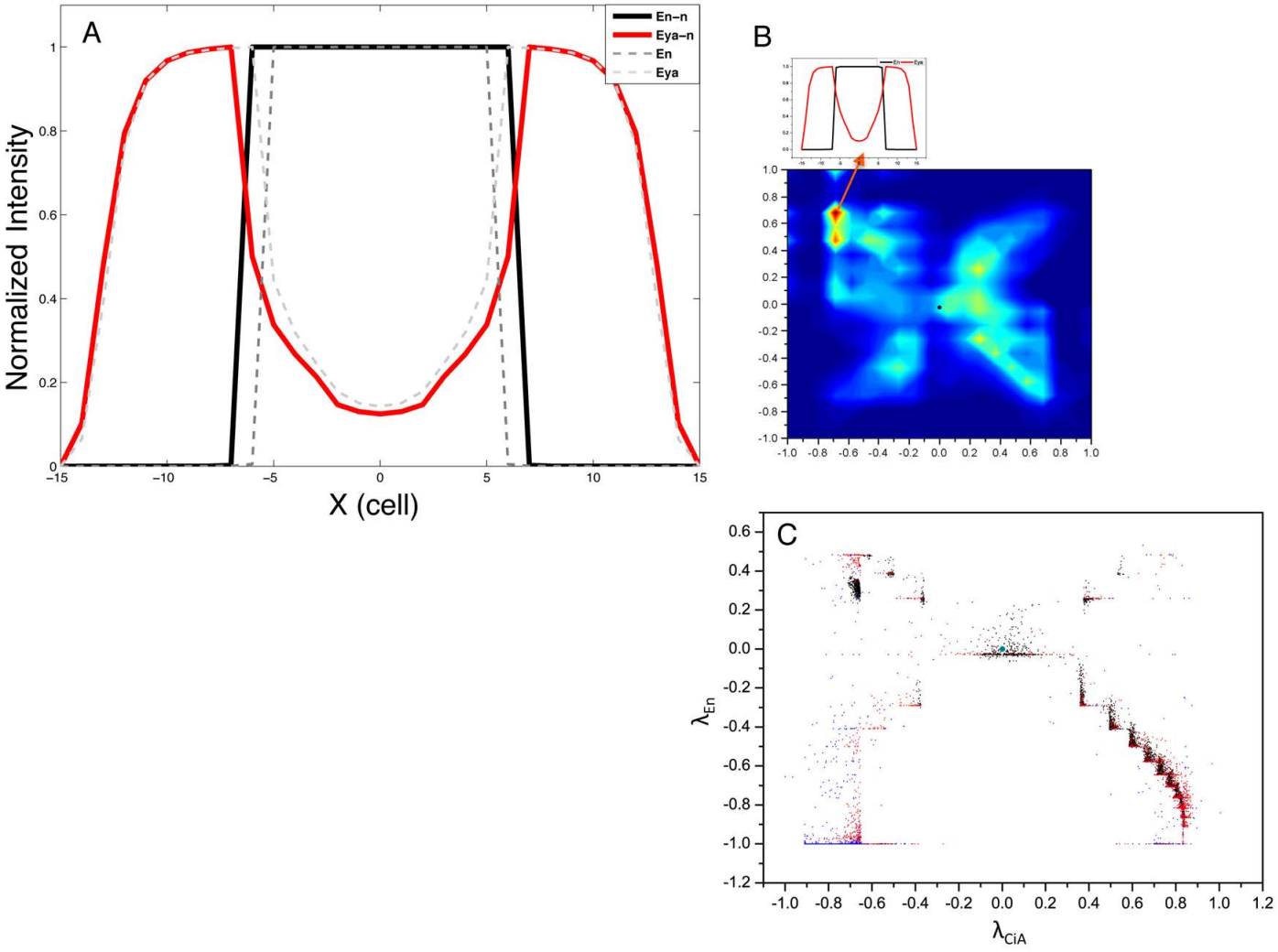

Fig. S7. Analysis of dense cluster pattern. (**A**,**B**) Noise effect on En and Eya profiles (A) over a specific pattern (B) situated in a dense cluster 'far', in global distance, from the wild type (0,0). (**C**) Projection of 10000 solution points corresponding to a randomized variation of all the sensitive parameters in ranges with complementary distance with value >0.8 (black dots), between 0.6 and 0.8 (red dots) and between 0.4 and 0.6 (blue dots). The projection is carried out on En and CiA distance patterns. There is significant overlap in the distribution of patterns generated by black, red and blue parameters, even though blue dots ('bad' parameters) tend to give patterns farther from (0,0).

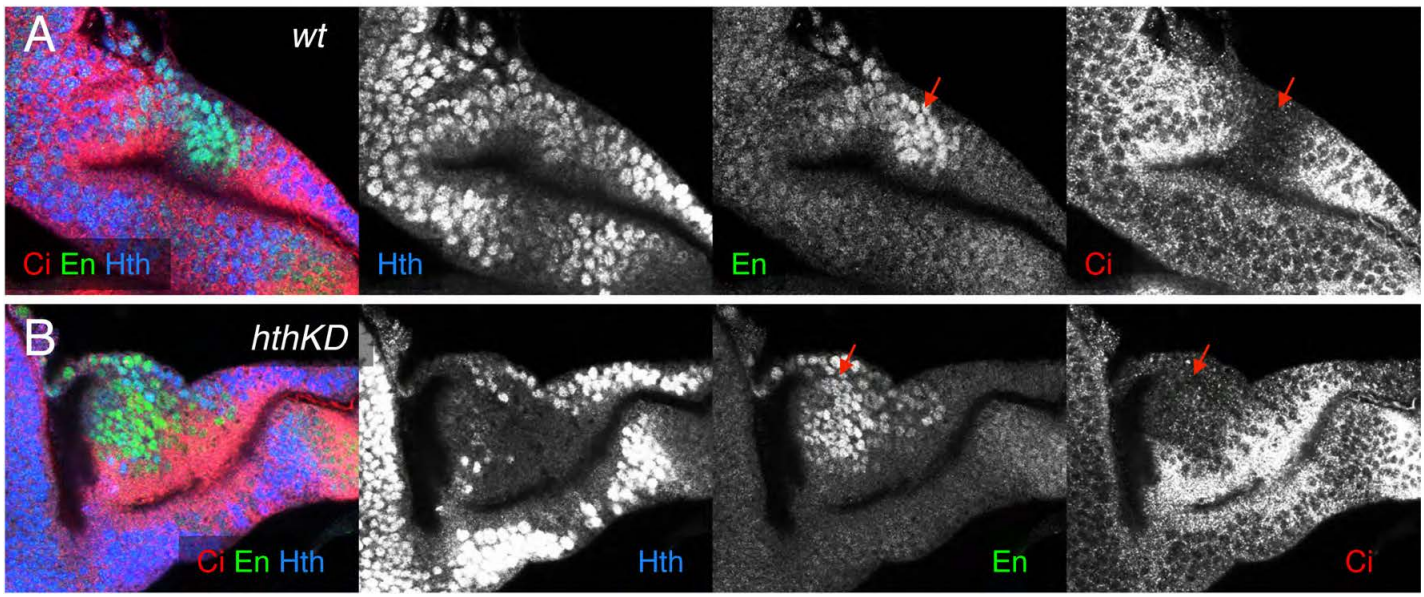

Fig. S8. *hth* regulates ocellar size without affecting *en* expression and its repression of the *hh* pathway. (**A**,**B**) Ocellar fields of control (A) and *oc2>hth(RNAi) (hthKD),* stained for Hth, En and Ci (B). In *hthKD* discs, Hth signal disappears in the whole ocellar field except for a few cells. In this genotype, *en* expression is detected at normal levels and Ci signal is downregulated in *en*-expressing cells. Red arrows indicate the En-expressing domain.

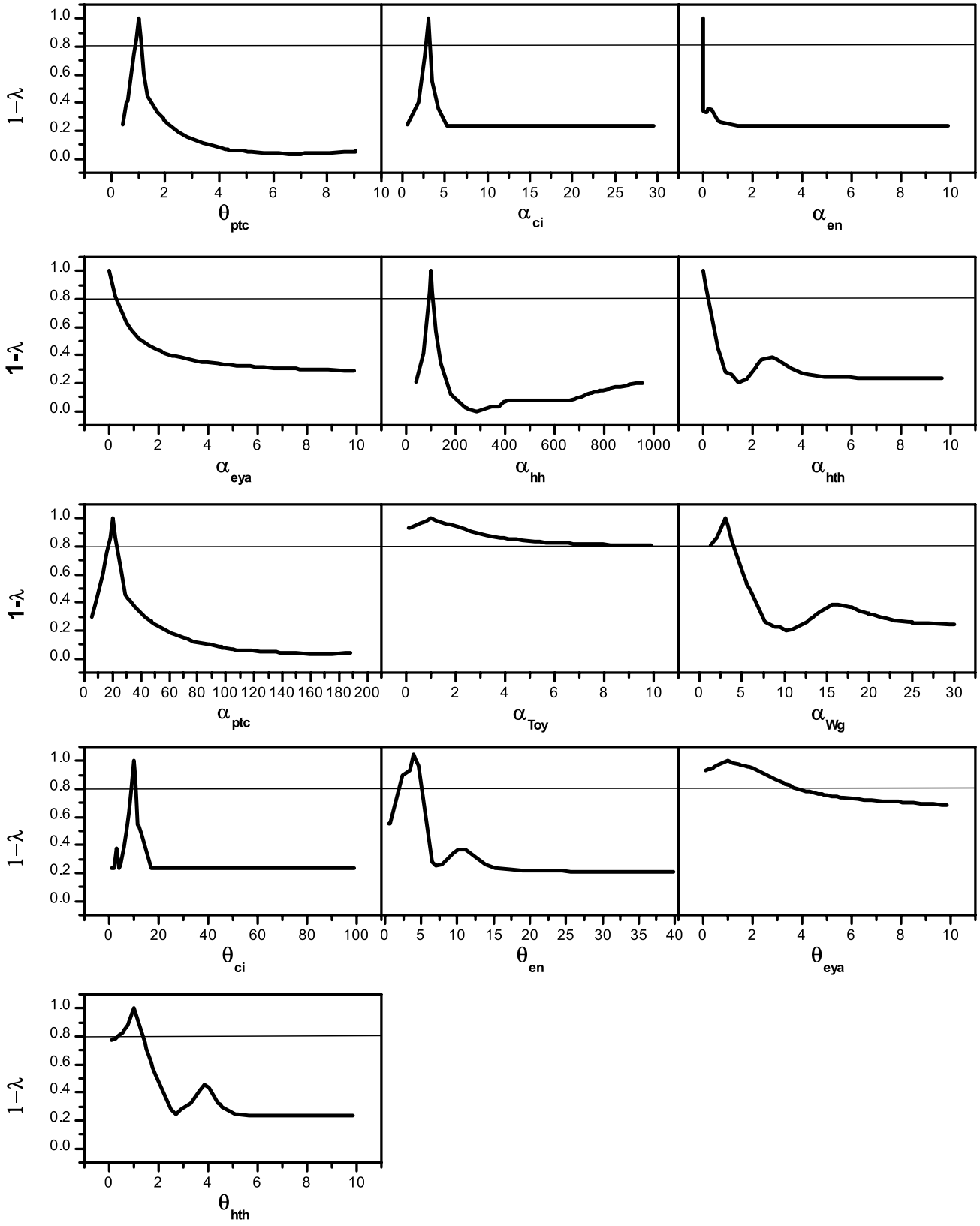

Fig. S9. Parameter sensitivity analysis plot. Goodness score (1–λ) for Eya pattern as a function of parameter values. λ is the Euclidean distance between the control Eya pattern and the pattern produced by a new value of the parameter. 1– λ was calculated for each parameter in a range of two orders of magnitude around the control value of the parameter. Goodness scores above 0.8 (line) are considered 'good' (i.e. within this range, the variation of the respective pattern results in Eya expression patterns closely resembling the control, or wild-type, pattern).

Table S1. Parameters and values used in the model. List of parameters used in the system with their control values. The list of parameters consists of different types: α_x for the basal transcription rates, β_x for the degradation rates, κ_x for the Hill equation transcriptional regulators, n_x for the Hill coefficients, θ_x for the translation rates; γ_{Ptc_Hh} for the protein complex formation of Ptc and Hh; the non-dimensional parameters κ_0, κ_{Ci}, κ_{En} and κ_{Ciptc} are different parameters used for changing the scale of different terms and D the diffusion coefficient. The values ranges correspond to a complementary distance to Eya wild-type pattern of (≥0.8), (≥0.6 and <0.8) and (≥0.4 and <0.6).

Parameter	Value	1-λ ≥ 0.8	0.6 ≥ 1-λ > 0.8	0.4 ≥ 1-λ > 0.6
α_{ci}	3	[2.75,3.27]	[2.24,2.75) ∪ (3.27,3.46]	[2.24,2.75) ∪ (3.27,3.46]
α_{en}	0	[0,0]	-	-
α_{eya}	0	[0,0.3]	(0.3,0.8]	(0.8,2.42]
α_{hh}	100	[91.2,106.6]	[80.2, 91.2) ∪ (106.6,117.6]	[67.03, 80.2) ∪ (117.6,132.96]
α_{hth}	0	[0,0.2]	(0.2,0.42]	(0.42,0.67]
α_{ptc}	20	[16.9,23.1]	[13.46, 16.9) ∪ (23.1,26.15]	[8.07, 13.46) ∪ (26.15,32.69]
α_{Toy}	1	[0.1,10]	-	-
α_{Wg}	3	[1.2,4.0]	(4.00, 5.06]	(5.06, 6.66]
β_{ci}	0.6	[0.1,6.0]	-	-
β_{CiA}	0.5	[0.37,0.64]	[0.20, 0.37) ∪ (0.64,0.81]	(0.81,1.00]
β_{CiR}	0.5	[0.4,0.65]	[0.26,0.4) ∪ (0.65,0.9]	(0.9,1.3]
β_{en}	0.1	[0.01,1.0]	-	-
β_{eya}	0.1	[0.01,1.0]	-	-
β_{Hh}	0.1	[0.03,0.22]	(0.22,0.34]	(0.34,0.72]
β_{hth}	0.1	[0.01,1.0]	-	-
β_{En}	0.5	[0.28,1.1]	[0.21,0.28) ∪ (1.1,1.55]	[0.14,0.21) ∪ (1.55,5]
β_{Eya}	0.1	[0.01,0.55]	-	-
β_{Hth}	0.5	[0.38,1.35]	-	-
β_{Ptc}	0.5	[0.38,0.67]	[0.3,0.38) ∪ (0.67,0.98]	[0.2,0.3) ∪ (0.98,1.63]
β_{ptc}	0.5	[0.05,5.0]	-	-
β_{PtcHh}	0.5	[0.43,0.57]	[0.36,0.43) ∪ (0.57,0.65]	[0.27,0.36) ∪ (0.65,1.04]
D	0.5	[0.4,0.57]	[0.24,0.4) ∪ (0.57,0.68]	[0.13,0.24) ∪ (0.68,2.6]
γ_{Ptc_Hh}	0.05	[0.045,0.11]	[0.04,0.045) ∪ (0.11,0.15]	[0.01,0.04) ∪ (0.15,0.25]
κ_0	10	[4.0,100]	-	-
κ_{Ci}	15	[12.1,19.6]	[9.3,12.1) ∪ (19.6,24.5]	[7.43,9.3) ∪ (24.5,51.9]
κ_{En}	2	[0.26,5.50]	[5.50,20]	-
κ_{Ciptc}	30	[19.87,40.0]	[10.89,19.87) ∪ (40,43.15]	[2,10.89) ∪ (43.15,74.3]
κ_{ci}	0.1	[0.01,0.216]	(0.216,0.40]	(0.4,0.78]
κ_{CiA}	2	[1.8,2.4]	[1.62,1.8) ∪ (2.40,2.72]	[1.11,1.62) ∪ (2.72,3.13) ∪ (3.81,8.99]
κ_{CiAen}	5	[3.46,9.95]	[2.80,3.46) ∪ (9.95,15.8]	[2.30,2.80) ∪ (15.8,50.0]
κ_{CiAeya}	7	[1.0,100]	-	-
κ_{CiAptc}	10	[6.26,21.2]	[3.72,6.26) ∪ (21.2,75.0]	[2.30,3.72) ∪ (75.0,100]
κ_{CiRen}	1	[0.76,1.24]	[0.49,0.76) ∪ (1.24,1.65]	[0.1,0.49) ∪ (1.65,2.27) ∪ (2.8,3.33]
κ_{CiRptc}	5	[1.7,18.4]	[0.8,1.7) ∪ (18.4,50]	-
κ_{DlEn}	0.2	[0.16,0.45]	[0.14,0.16) ∪ (0.45,0.91]	[0.01,0.14) ∪ (0.91,10]
κ_{Enci}	0.5	[0.1,1.1]	-	-
κ_{Enptc}	25	[5.1,250]	-	-
κ_{Eya}	20	[3.38,200]	-	-
κ_{Eyahth}	8	[0.8,80]	-	-
κ_{Htheya}	2	[1.58,5.0]	-	-
κ_{PH}	0.13	[0.11,0.14]	[0.1,0.11) ∪ (0.14,0.17]	[0.07,0.1) ∪ (0.17,0.24]

κ_{Wg}	2	[1.66,3.40]	-	-
n_{ci}	1	[1,2]	[3,100]	-
n_{CiA}	4	[4,5]	3 ∪ [6,10]	2 ∪ [11,100]
n_{CiAen}	1	[1,1]	[2,100]	-
n_{CiAeya}	9	[1,100]	-	-
n_{CiAptc}	1	[1,100]	-	-
n_{CiRen}	4	[4,4]	3,5	-
n_{CiRptc}	1	[1,5]	[6,100]	-
n_{En}	10	[7,100]	-	-
n_{Enci}	12	[4,100]	-	-
n_{Enptc}	5	[1,100]	-	-
n_{Eya}	2	[2,100]	-	-
n_{Hth}	2	[1,5]	-	-
n_{PH}	1	[1,1]	-	-
n_{Wg}	2	[2,3]	-	-
θ_{ci}	10	[9.12,10.6]	[7.58,9.12) ∪ (10.6,11.7]	[6.00,7.58) ∪ (11.7,14.3]
θ_{en}	4	[2.12,5.0]	[1.00,2.12) ∪ (5.00,5.50]	[0.62,1.00) ∪ (5.50,6.25]
θ_{eya}	1	[0.1,3.88]	[3.88,10.0]	-
θ_{hth}	1	[0.4,1.33]	[1.33,1.74]	[1.74,2.20) ∪ (3.60,4.10]
θ_{ptc}	1	[0.89,1.12]	[0.71,0.89) ∪ (1.12,1.19]	[0.55,0.71) ∪ (1.19,1.47]

Table S2. Initial condition for each system variable.

Variable	Description	Initial Condition
Hh	Hh concentration	0.1 μM
ptc	ptc concentration	0.1 μM
Ptc	Ptc concentration	0.1 μM
PtcHh	PtcHh complex concentration	0.1 μM
ci	ci concentration	0.1 μM
CiA	CiA concentration	0.1 μM
CiR	CiR concentration	0.1 μM
en	en concentration	0.01 μM
En	En concentration	0.01 μM
eya	eya concentration	0.1 μM
Eya	Eya concentration	0.1 μM
hth	hth concentration	0.75μM*
Hth	Hth concentration	1.5μM**

* Initial *hth* concentration correspond to its stationary value in the absence of Eya repression ($[hth]=\kappa_0\beta_{hth}\left(\alpha_{hth}+\alpha_{Wg}/k_{Wg}^{n_{Wg}}\right)$).** Initial Hth concentration corresponds to its stationary value ($[Hth]=\theta_{hth}[hth]/\beta_{hth}$). See table 1 for parameter values.

APPENDIX 1 FOR

A Hh-driven gene network controls specification, pattern and size of the *Drosophila* simple eyes.

D Aguilar-Hidalgo[§1,2], MA Domínguez-Cejudo[§1], G. Amore[3], A Brockmann[1,4], MC Lemos[2], A Córdoba[2], F Casares[1]*.

§- Equal contribution authors, listed in alphabetical order.

1- CABD (CSIC-UPO-Junta de Andalucía), Sevilla, Spain.
2- Condensed Matter Physics Dept. (U. Sevilla), Sevilla, Spain.
3- Stazione Zoologica Anton Dohrn, Napoli, Italy.
4- Current address: University of Konstanz, Germany

* Corresponding author: fcasfer@upo.es

Design and implementation of the ocellar mathematical model.

The design of this model is based on differential equations of the reaction-diffusion type. This model consists of 13 equations, one for each system variable (genes transcription and protein production) in a row of 31 cells with a symmetrical distribution of cells centered on the morphogen source (5 middle cells). Globally, the mathematical model comprises 403 ordinary differential equations (ODEs).

The design of the equation system follows the formulation paradigm used by von Dassow et al. (von Dassow et al., 2000). This methodology distinguishes between mRNA transcription and protein translation. Translation is described as linear terms of production and degradation. Transcriptional regulation is described with non-linear terms, either positive or negative, in the form of compound Hill equations. The specific form of these type of terms is $\phi(X\psi((Y,k_2,n_2),k_1,n_1)$, where

$$\phi(X,k,n)=\frac{X^n}{k^n+X^n} \qquad \text{(s1)}$$

and

$$\psi(Y,k,n)=\left(1-\frac{Y^n}{k^n+Y^n}\right), \qquad \text{(s2)}$$

so

$$\phi(X\psi(Y,k_2,n_2),k_1,n_1)=\frac{X^{n_1}\left(1-\frac{Y^{n_2}}{k_2^{n_2}+Y^{n_2}}\right)^{n_1}}{k_1^{n_1}+X^{n_1}\left(1-\frac{Y^{n_2}}{k_2^{n_2}+Y^{n_2}}\right)^{n_1}} \qquad \text{(s3)}$$

The ocellar model also contains autoregulations. In these cases, the equation term is described as a simple sigmoid in the form $\phi(X,k,n)$.

Parameter Sensitivity Analysis: one-by-one analysis.

Once a wild type set of parameter values had been found we tested whether these values are unique or if, on the contrary, it is possible to find different parameter sets that also lead to correct behaviors. One would expect that this latter option to be found, as organ development should be evolutionarily prepared to remain relatively constant in the face of fluctuations (i.e. to be robust) some of which may affect the biochemical properties of the gene networks controlling this development.

To analyze this issue, we carried out a parameter sensitivity analysis. The major problem we face is, once more, the large number of parameters. Therefore, we proceeded in two phases. In the first phase, we explored the parameter space modifying just one dimension (parameter) at a time; the rest of parameters are fixed to the "control" or wild type values. To do this, we defined a searching range for each parameter of two orders of magnitude around the "control" value for the wild type pattern. The resulting pattern was compared to the wild type and a goodness score obtained. This score represents the Euclidean distance (λ) between the Eya wild pattern and the Eya pattern drawn by the new set of parameters. To calculate the score, it was considered that both, the wild type (A) and the new (B) Eya patterns are described by two 31 component vectors (one component for each cell in the system). Then, the distance between these two vectors is defined as their Euclidean norm.

$$\lambda = \left|\left|\overrightarrow{AB}\right|\right| = \sqrt{\sum_i \left(b_i - a_i\right)^2} \qquad \text{(s4)}$$

where a_i and b_i are the components of vectors A and B, respectively.

In Sup. Figure S9 the distance distributions (considered as complementary distance, 1- λ) for all the system parameters are shown. From this analysis it is possible to extract important information about which parameters are more sensitive or more insensitive to variations away from the control parameter

values. In fact, some parameters can be considered quite insensitive, as their distances do not undergo significant changes.

A complementary distance value of 0.8 was selected as a "goodness" threshold, as every pattern checked for a parameter set with a complementary distance value equal or higher to this value fits the target ocellar pattern.

Following this "goodness" threshold, every parameter whose distance distribution falls below 0.8 is considered "sensitive" (33 parameters); and parameters whose distance distribution always remains above this threshold are considered "insensitive" (28 parameters). There are some parameters among the sensitive ones that are extremely sensitive as their variation range above the distance threshold is really small. The most restrictive parameter is α_{en}, which is responsible of the basal transcription of gene *en*. The wild type condition makes this parameter null. The sensitivity analysis predicts that this parameter should remain null or otherwise the distance value would fall.

At this point, we have determined which are the sensitive parameters and which can be freely varied without major consequence in the patterning. We have also established which are the ranges within which each sensitive parameter can be modified while the pattern obtained still remains within a given goodness distance interval.

Parameter Sensitivity Analysis: multiparametric analysis.

In the second phase we reconsidered the full parameter space exploration but eliminating from this study the insensitive parameters, and restricting the value ranges to those that give "good" patterning. Although these restrictions can be made, the resulting pattern is not assured to be "good", as the parameter space is still vast and the high complexity of the system might provide really "far" distance values just when modifying two parameters simultaneously. In order to be able to distinguish if the system can give "bad" patterns from "good" parameter values and, if "bad" parameter values always return "bad" profiles, a goodness scaling can be prepared. From the results in the parameter sensitivity analysis, we calculated, in addition to the "good" ranges, the parameter value ranges for distances between 0.6 and 0.8 ("medium"), and between 0.4 and 0.6 ("bad").

A total number of 10000 runs were obtained distributed in 6000 “good”, 3000 “medium” and 1000 “bad” randomized parameter values. With this 10000 parameter sets the distance for all the patterns of the system (one per variable) was calculated. In this way, each parameter set defines a point in a 13-dimensions space, each dimension being one of the model’s variables.

2D representation of the parameter sensitivity analysis

In order to represent the analysis, it was important to define a method to calculate a global distance in this hyperspace for visualizing the results in 2D. In the first place, the Euclidean norm does not distinguish sign, that is, it is not possible to know which of the patters, wild type and randomized, is bigger. So before calculating the norm it was determined which pattern defines a larger area under the curve. Thus, the distance between the two patterns is positive if the wild type pattern defines a larger area than the randomized pattern.

If we consider a 2D representation of the distance with sign, the wild type pattern would be placed in point (0,0). It is possible to plot just the distance from two different patterns out of 13 but this would just show the projection of the 13-dimentional points into 2D, and this projection may change depending on the two dimensions chosen for the plot. A method was implemented to visualize all the projections at one time.

To do so, first the normalized distance is divided into 0.1 length segments. Then the number of points in each 0.1x0.1 square for each projection of two variables was counted. The counting considered order, that is, the projection A-B is the same as B-A and just one of them is counted. This process is repeated for all the squares in the grid and for all the combinations of dimension pairs.

The result of this method can be seen in Figure 7F and Suppl. Fig. S7B. This plot represents the density of patterns from the 10000 randomized runs distributed relative to their distance from the wild type pattern. Therefore, this representation is a sort of phenotypic map produced by the network using the random sets of parameters.

Biological simplifications: The rationale for not including proliferation in the model, at least in this study, is the following: The development of the ocelli spans the second half of L3, that is, approximately 24 hours at 25^{o}C. Our estimate of the doubling rates in the eye field is about 13 hours (CS Lopes and FC, unpublished). Since the ocellar region does not express neither *eyg* nor *upd,* genes involved in stimulating cell proliferation in the eye field downstream of *Notch,* we expect the doubling rate in the ocellar field to be 13 hours or lower, therefore justifying our assumption.

Biological data used in the modeling of the Hh signaling pathway, including *en.*

The nuclear transducer of the Hh signaling pathway is encoded by *ci. ci* gives rise to an uncleaved form of Ci. In the absence of signal, Ci is processed proteolitically (and thus irreversibly) into a transcriptional repressor, CiR (Aza-Blanc et al., 1997; Methot and Basler, 1999). However, in the presence of signal, Ci is converted into a transcriptional activator, CiA. Hh signaling strength depends on the ratio between bound (to Hh) and unbound Ptc (Casali and Struhl, 2004), so that the higher this ratio, the more CiA (and the less CiR) is produced. CiA and CiR are thought to bind to similar DNA sequences in vivo to activate and repress, respectively, a similar set of targets genes. These include *en* and the Hh receptor *ptc* (Alexandre et al., 1996; Methot and Basler, 1999; Biehs et al., 2010). Therefore, in our model we assume a similar regulation for *ptc* and *en* in the ocellar region. In addition, *ci* basal transcription can be repressed by En (Schwartz et al., 1995). Another key element in the Hh pathway is the regulation of *ptc. ptc* transcription is positively regulated by Hh signaling and negatively by En. Then, the Ptc protein can bind to Hh. The Ptc:Hh complex is degraded after endocytosis, thereby making this association step irreversible.

Analysis of the Hh gradient steady state.

It is known that *hh* transcription is restricted to the interocellar region, known as *hh*-expressing zone. In this region $\delta(x) = 1$.

Once the morphogen gradient reaches its steady state ($t = t_{std}$) and Ptc is constant ([Ptc]), we have:

$$\left.\frac{\partial Hh}{\partial t}\right|_{t=t_{std}} = 0 \qquad \text{(s5)}$$

and,

$$D\frac{\partial^2 Hh}{\partial x^2} + \alpha_{hh} - \gamma_{Ptc\_Hh}[Ptc]\cdot Hh - \beta_{Hh}Hh = 0 \qquad \text{(s6)}$$

or,

$$D\frac{\partial^2 Hh}{\partial x^2} + \alpha_{hh} - \left(\gamma_{Ptc\_Hh}[Ptc] + \beta_{Hh}\right)Hh = 0 \qquad \text{(s7)}$$

The solution to this equation is:

$$Hh(x) = Hh_0 e^{-\frac{x}{\lambda}} - \frac{\alpha_{hh}}{\gamma_{Ptc\_Hh}[Ptc] + \beta_{Hh}} \qquad \text{(s8)}$$

The parameter $\lambda = \sqrt{D/\left(\gamma_{Ptc\_Hh}[Ptc] + \beta_{Hh}\right)}$ is known as decay length, which corresponds to the distance at which the morphogen concentration decays by a factor of *1/e*.

From Fick's first law we can assert that the morphogen production rate is given by:

$$\alpha_{hh} = -\frac{\partial Hh}{\partial x} \qquad \text{(s9)}$$

The flux direction is from higher concentration to lower concentration regions, being the flux a magnitude proportional to the gradient concentration. Thereby:

$$\alpha_{hh} = Hh_0\sqrt{D\left(\gamma_{Ptc\_Hh}[Ptc] + \beta_{Hh}\right)} \quad \text{at} \quad x = 0 \qquad \text{(s10)}$$

then,

$$Hh_0 = \frac{\alpha_{hh}}{\sqrt{D\left(\gamma_{Ptc\_Hh}\left[Ptc\right]+\beta_{Hh}\right)}} \tag{s11}$$

and,

$$Hh(x) = \frac{\alpha_{hh}}{\sqrt{D\left(\gamma_{Ptc\_Hh}\left[Ptc\right]+\beta_{Hh}\right)}} e^{-\frac{x}{\sqrt{D/\left(\gamma_{Ptc\_Hh}\left[Ptc\right]+\beta_{Hh}\right)}}} - \frac{\alpha_{hh}}{\gamma_{Ptc\_Hh}\left[Ptc\right]+\beta_{Hh}} \tag{s82}$$